OBSERVATIONAL COSMOLOGY:

GALAXY CLUSTERS AND THE INTRACLUSTER MEDIUM

Credits: B. Sartoris, A. Saro

A.A. 2025/2026 | Matteo Costanzi - University of Trieste / INAF

STRUCTURE FORMATION: DARK MATTER HALOS

In the LCDM scenario, structures grow *hierarchically*: Small overdensities are able to overcome the cosmological expansion and collapse first, and the resulting dark matter "halos" merge together to form larger halos which serve as sites of galaxy and galaxy cluster formation

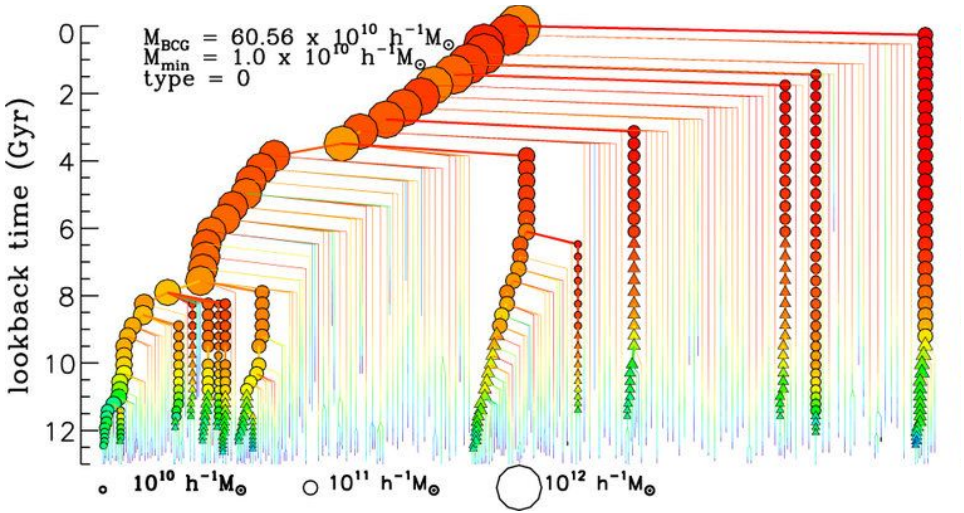

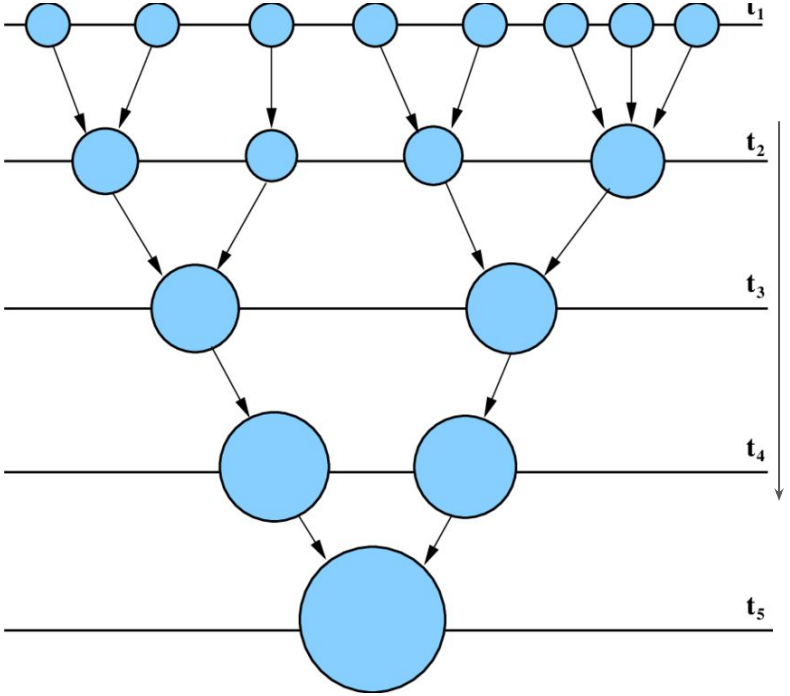

GALAXY CLUSTERS

- Most massive bound objects in the Universe:
  - $M \simeq 10^{14} - 10^{15}\ M_{\odot}$ and $R \simeq 1 - 5$ Mpc
- Form from the highest density peak of the initial matter density field
  - Preferentially located at the knots of the LSS
- Firstly identified as large concentration of (passive) galaxies with large velocity dispersion:
  - 100-1000 galaxies, $\sigma_v \simeq 500 - 1000$ km/s

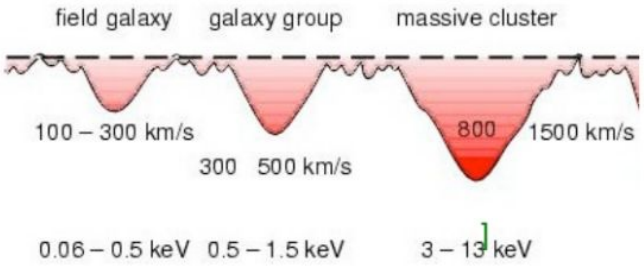

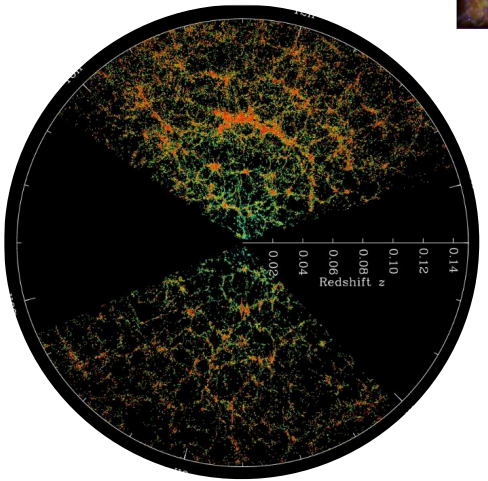

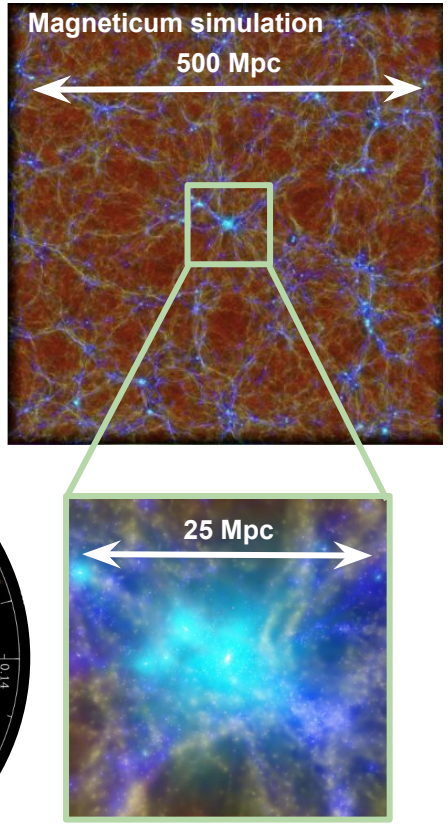

From Hirschmann+2014

GALAXY CLUSTERS

- **Multi-component systems:**
  - **Galaxies and stars (~5%), ICM (~15%), DM (~80%)**
  - **Allow to detect clusters at different wavelengths**
  - **Perfect astrophysical laboratory to study: galaxy evolution, gas and plasma astrophysics**

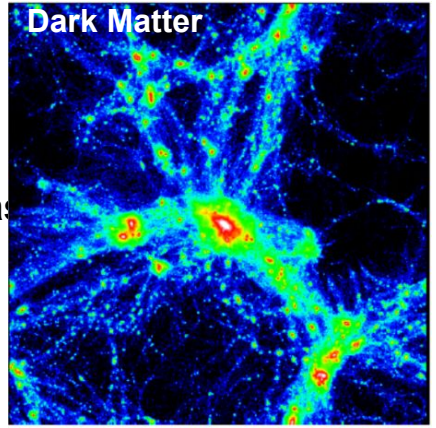

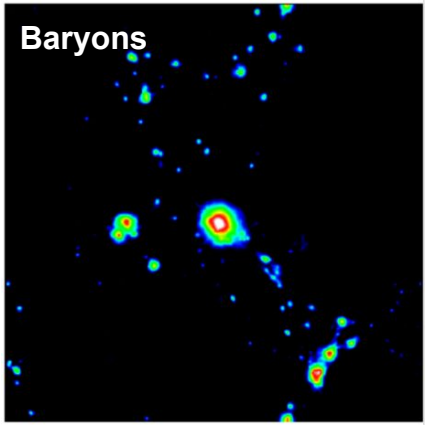

OPTICAL

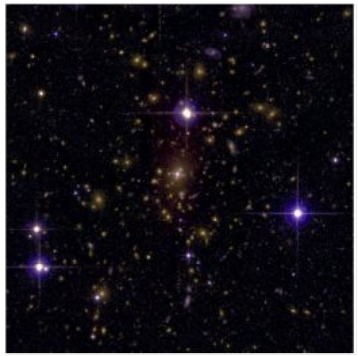

RICHNESS, LENSING EFFECTS

X-RAYS

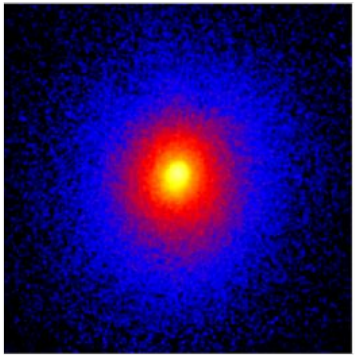

LUMINOUS AND EXTENDED X-RAY SOURCES

MICROWAVES

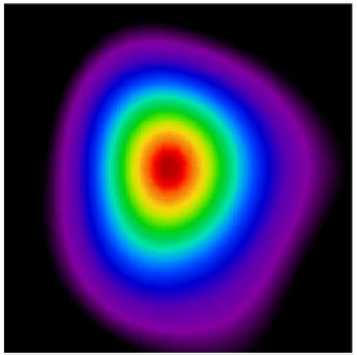

SUNYAEV-ZEL'DOVICH EFFECT

CLUSTER BOUNDARY

Operational definition:

- **The cluster border is not a well-defined quantity: clusters are not closed spheres, however it is convenient to define a cluster as the mass enclosed in a radius corresponding to a fixed overdensity Δ.**
  - **Δ is defined as the overdensity with respect to the mean or the critical density of the Universe at the cluster redshift.**

$$M_{\Delta} = \frac{4\pi}{3} r_{\Delta}^{4} \rho_{m/cr} \Delta$$

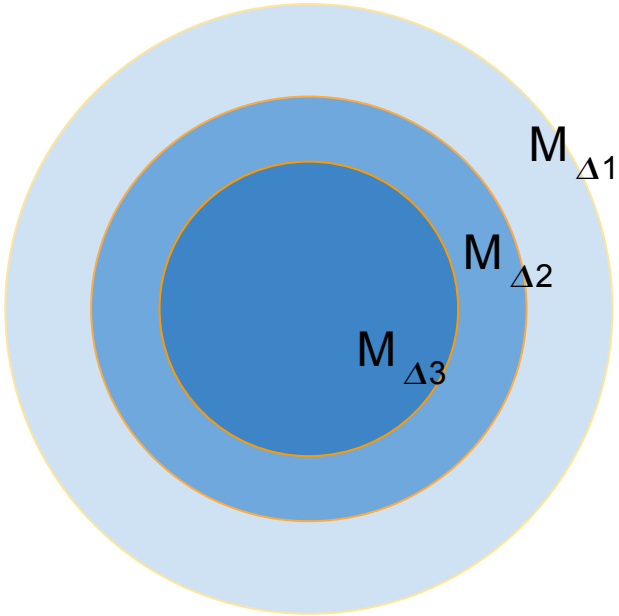

CLUSTER BOUNDARY

Splashback radius:

- **The cluster edge can be defined by the orbital dynamics of the matter within the cluster.**
- **The splashback radius represents the location of the first orbital "turnaround", i.e. the maximum distance a particle reaches after its first passage through the cluster.**
- **At the location of the Splashback radius is expected a rapid decline of the density profile.**

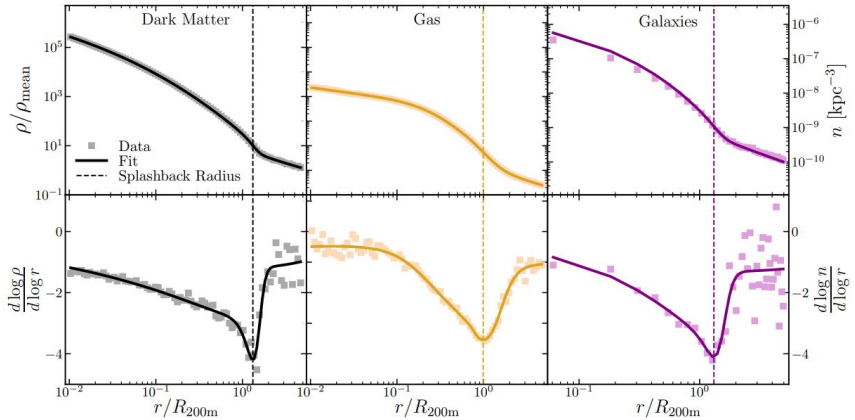

DM, gas and galaxy density profiles and splashback radius from TNG hydrosim (O'Nail+20)

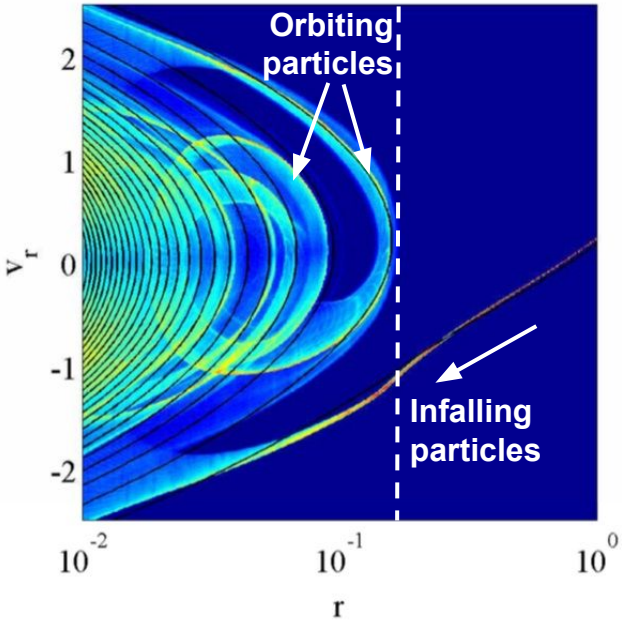

Phase space diagram showing velocity of dark matter particles as a function of radius in a halo in idealized simulation

INTRACLUSTER MEDIUM

ICM:

- **Hot (10^7 - 10^8 K), optically thin plasma, that permeates the space between galaxies within a GC**
- **Result of the gas infall into the dark matter halo gravitational well**
- **The gas is heated primarily through accretion shocks and adiabatic compression during the hierarchical assembly of the cluster**
- **AGN feedback and sloshing of the ICM plasma during mergers with subclusters prevent the central ICM from cooling**
- **Fossil record of the chemical enrichment of the Universe: the deep gravitational potential wells of clusters lock metals produced by member galaxies**

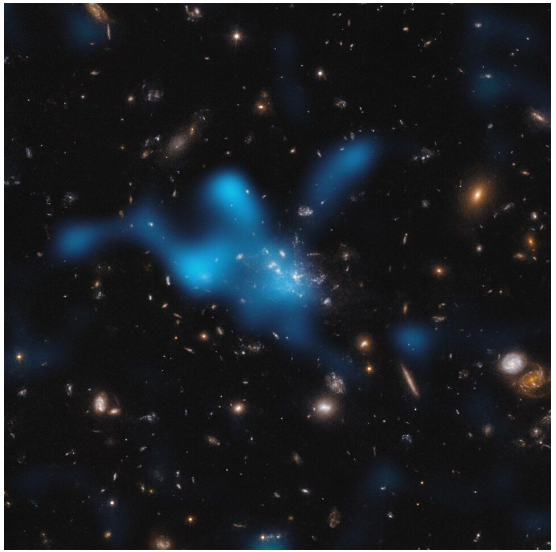

The overlaid blue cloud illustrates the intracluster medium around the Spiderweb Galaxy. The hot gas was detected with the Atacama Large Millimeter/submillimeter Array (ESO/Di Mascolo et al.; HST: H. Ford).

INTRACLUSTER MEDIUM

ICM:

- **Density: 10^{-3} - 10^{-1} particle/cm^3**
- **Compositions: fully ionized plasma; mostly H and He, with metallic traces (Fe, O, Ne, Si)**
- **Magnetic field: Weak but pervasive (~0.1 to 10 μG), influencing particle transport. The field varies on scales from 0.1 to 10 kpc.**
- **Emission: primarily via X-ray**
  - **Free-free: Thermal Bremsstrahlung radiation ~90% of the luminosity → continuum**
  - **Free-bound: recombination → continuum**
  - **Bound-bound: de-excitation radiation → line emission**

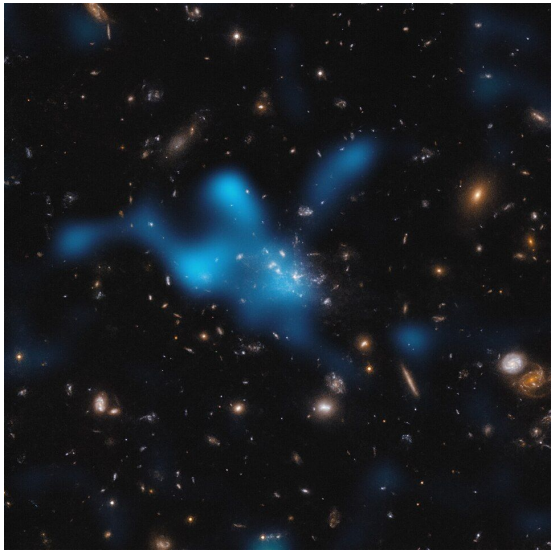

The overlaid blue cloud illustrates the intracluster medium around the Spiderweb Galaxy. The hot gas was detected with the Atacama Large Millimeter/submillimeter Array (ESO/Di Mascolo et al.; HST: H. Ford).

ICM X-RAY SPECTRUM

Bremsstrahlung spectrum:

- **Bremsstrahlung X-ray emissivity:**

$$\epsilon_\nu \equiv \frac{\mathrm{d}L}{\mathrm{d}V\mathrm{d}\nu} \propto n_e^2 g(\nu, T) T^{-1/2} \exp(-h\nu/k_B T)$$

- **Proportional to the square of the gas density**
- **The overall normalization scales as ∝ $T^{-0.5}$**
- **Exponential thermal cut-off at the electron's kinetic energy ($k_B T$)**
  - **The location of the cut-off provides strong constraints on the ICM temperature**

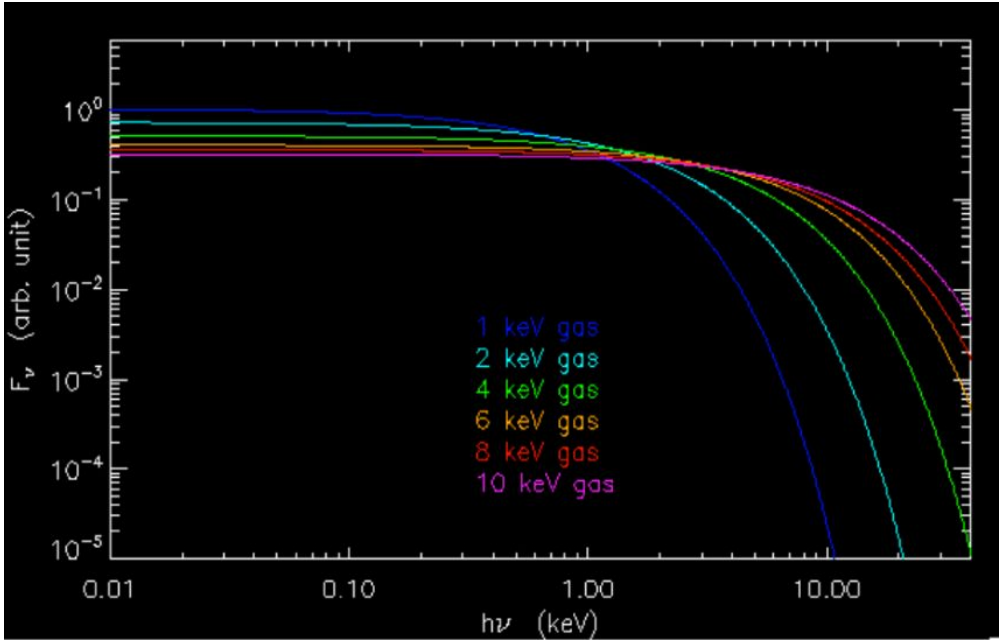

Bremsstrahlung X-ray spectrum for hot gas at different temperatures

ICM X-RAY SPECTRUM

Observed ICM spectrum:

- **Recombination lines: "edges" in the lower temperature spectra (e.g. 1 keV line around 0.5–1 keV)**
  - **Above ~6 keV the cross-section for electron capture drops significantly and the "edges" get smeared out**
- **Emission lines:**
  - **Strength of the line depends on temperature (e.g. Fe K-α @ k6.7 eV)**
  - **Soft X-ray lines (0.5-2 keV): due to elements like O, Ne, Mg → present only if the metals are not fully ionized (<6 keV)**

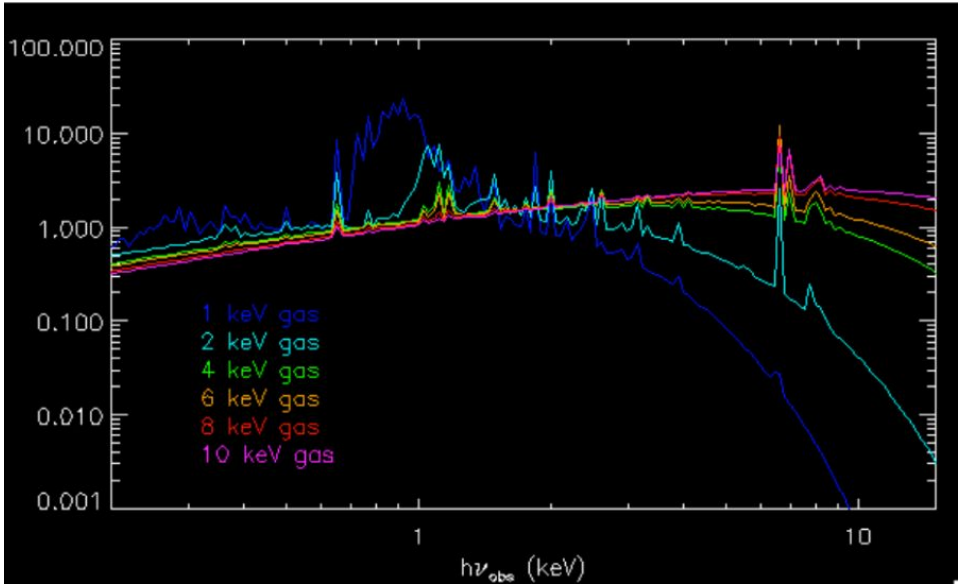

ICM X-RAY SPECTRUM

Observed ICM spectrum:

- **Emission lines:**
  - **Diagnostic for ICM metallicity**
  - **Most prominent signature of the metal enrichment is the Fe K-line complex at 6.7 keV**
  - **Fe-K is the only accessible line at high-z → only mean to determine cluster redshift from X-ray data**
  - **Iron L-shell Complex (at ~1 keV): It is caused by hundreds of overlapping emission lines from partially ionized Fe atoms (Fe^{16} to Fe^{23})**
  - **"Soft" Elements (0.5 – 3.0 keV) lines: useful diagnostic for star formation history**

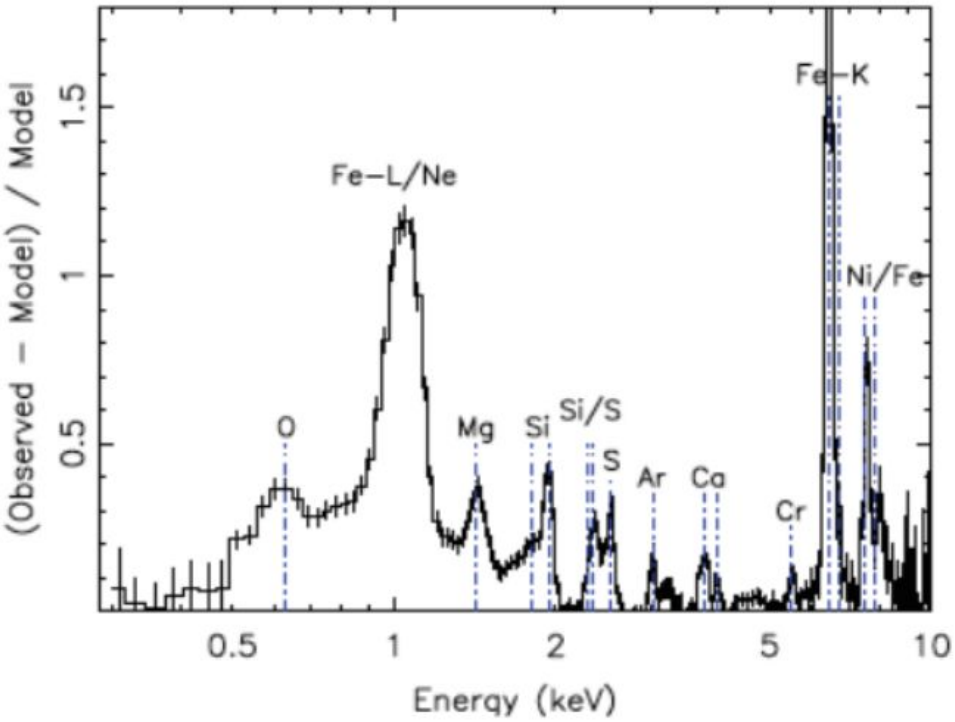

Residual Spectrum: By removing the smooth continuum , we are left with a clear view of the **chemical enrichment** of the ICM

ICM X-RAY SPECTRUM

In modern X-ray astronomy (using satellites like Chandra or XMM-Newton), the spectral resolution isn't always high enough to see the individual lines.
Observed spectra are fitted to plasma radiation codes which includes all the known emission processes

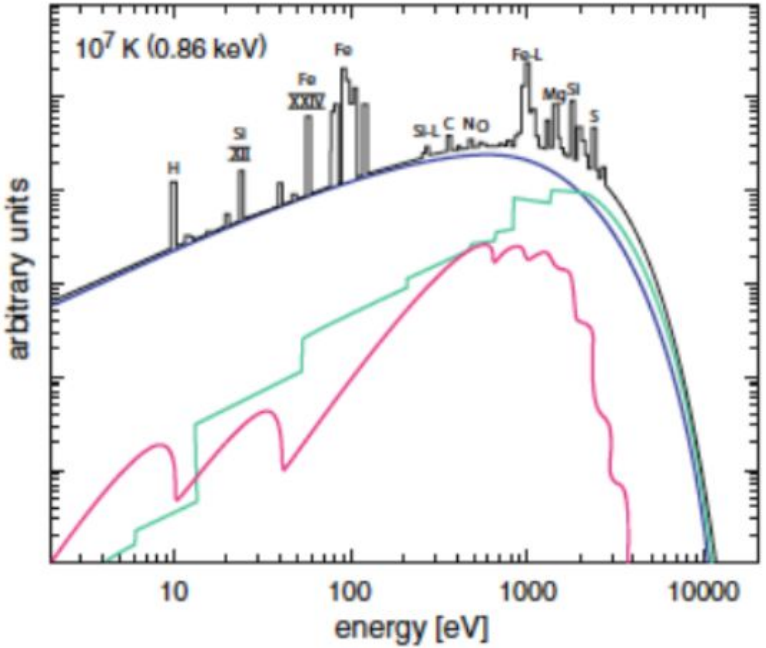

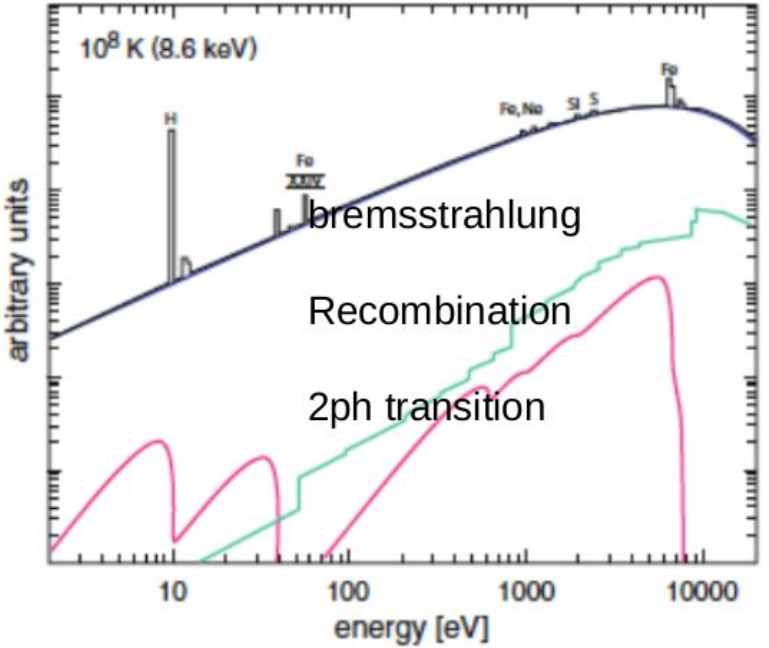

ICM: TEMPERATURE PROFILE

- **By fitting observed X-ray spectra measured at different radii with tabulated spectral emission convolved with the instrument response, is it possible to derive the ICM temperature profile**

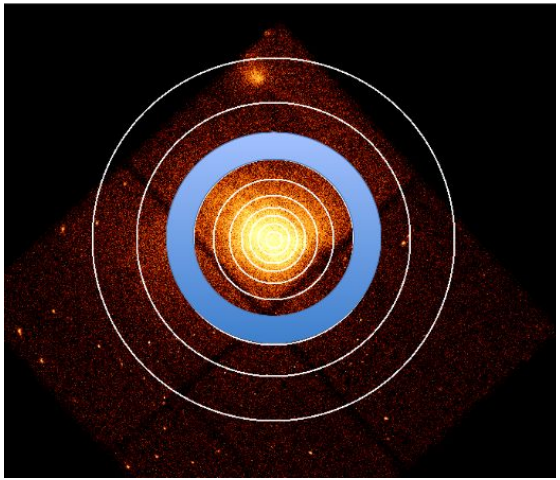

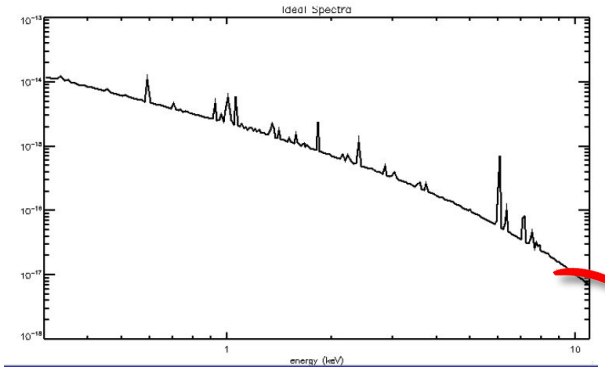

Ideal spectrum

Convolution with instrument response

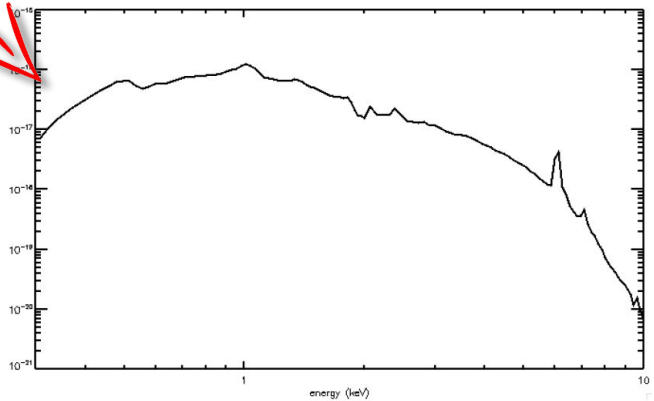

ICM: TEMPERATURE PROFILE

Temperature profile:

- **Expected cooling curve for a gas in hydrostatic equilibrium**
- **At large radii, R > 0.2 R_{200}, the normalized profile looks self-similar**
  - **the same gravity-driven physics shape all clusters**
- **Some profiles show a significant drop in temperature toward the core (Cool Core) while other profiles are ~flat (Non-Cool Core)**
- **To accommodate the variety of temperature profiles Vikhlinin et al 2006 introduced the parametric model**

$$T_{3D} = T_0 \frac{(r/r_t)^{-a}}{[1+(r/r_t)^b]^{c/b}} \frac{x + T_{min}/T_0}{x+1}$$

Temperature profiles from *XMM-Newton* observations (Pratt+06)

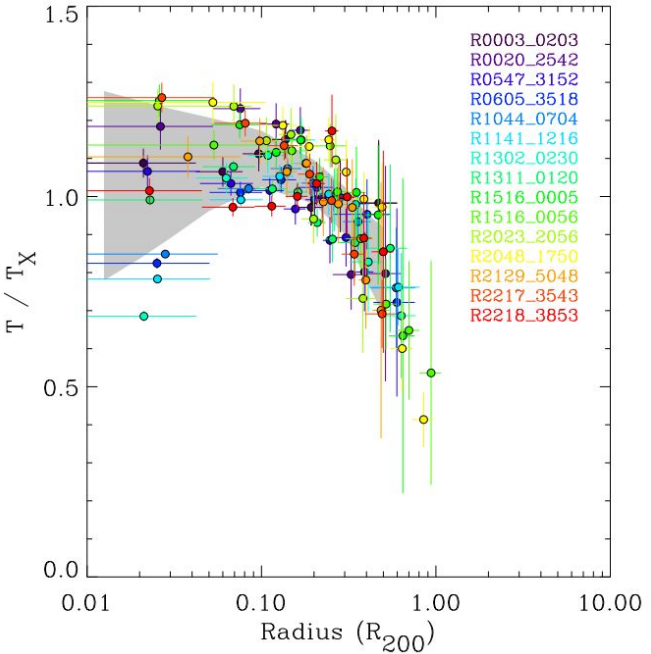

ICM: METALLICITY PROFILE

- The metallicity profile show a sharp rise toward the center ($R/R_{500} < 0.2$), reaching ~solar value in the inner core.
  - The peak is driven by the metal production of the central galaxy
- At large radii ($R/R_{500} > 0.3$) the profiles flatten out to a constant value A~0.3
  - this value is consistent across different clusters and extends so far out in radius that it suggests early enrichment (z ≃ 2-3) of the medium

Mean metallicity profiles from a sample of 207 nearby galaxy groups and clusters observed with XMM-Newton (Lovisari&Reiprich 2019)

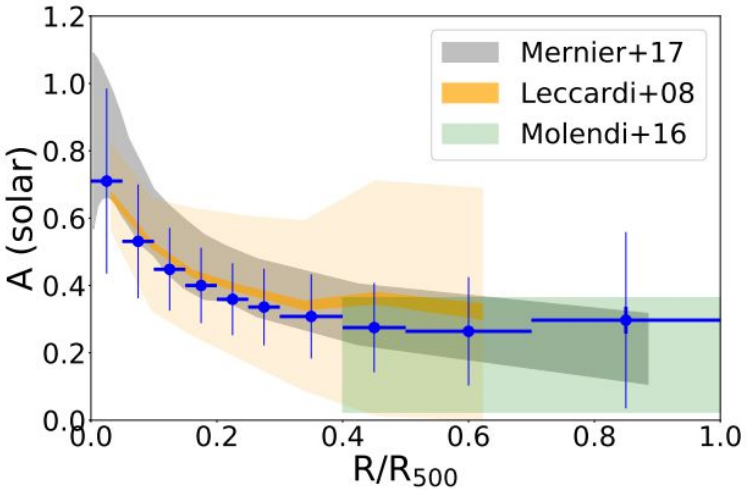

ICM: METALLICITY PROFILE

- **The evolution of the Fe abundance with redshift confirm early enrichment of the medium**

Mernier et al 2018

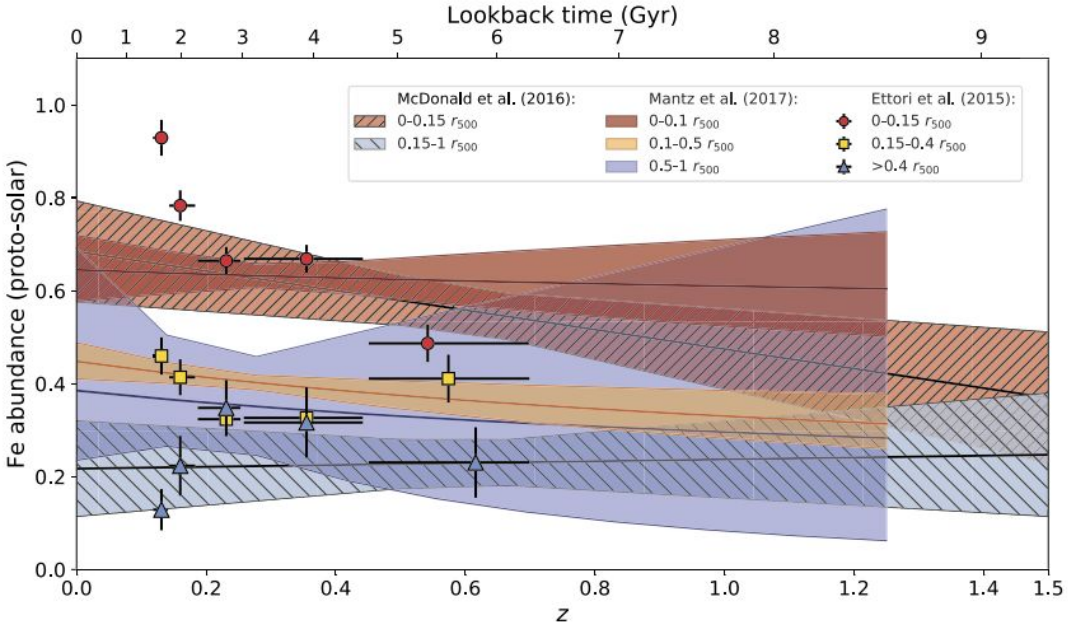

Fig. 8 Redshift evolution of the Fe abundance within different radial bins in cool-core clusters, compiled from recent works. For clarity, the scatter of the measurements are not shown. All the abundances are rescaled with respect to the proto-solar values of Lodders et al. (2009)

ICM: METALLICITY PROFILE

- **The large scatter observed in this relation is strongly associated with the dynamical state of the systems:**
  - **Relaxed systems have on average a higher metallicity in the core than disturbed objects.**
  - **The metallicity of disturbed systems is also higher in the center but at much lower values than what is observed for relaxed objects.**

- **This finding is consistent with the picture that cluster mergers mix the abundance distribution by inducing large scale motions.**

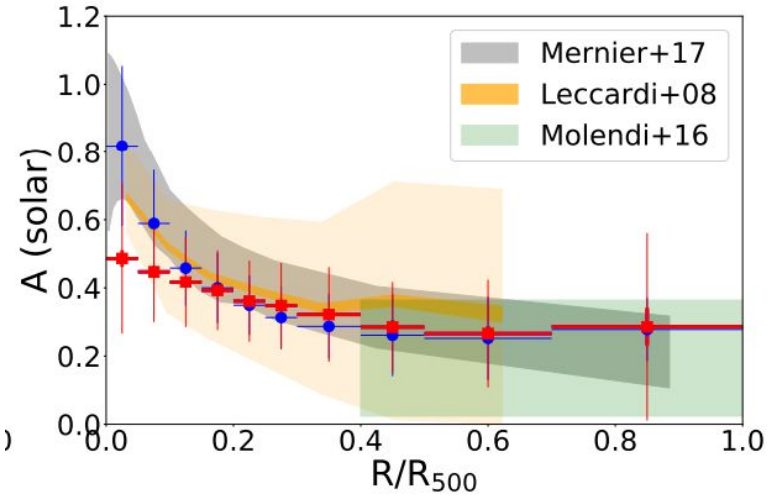

Mean metallicity profiles from sample of 207 nearby galaxy groups and clusters observed splitted in relaxed (blue) and disturbed (red) systems (Lovisari&Reiprich 2019)

GAS DENSITY PROFILE

The β model:

- **Assuming an isothermal sphere, equating the Jeans and HE mass estimates leads to the definition of the β parameter.**

$$M(r) = -\frac{\sigma_r^2 r}{G}\left\{\frac{d\ln\rho}{d\ln r}\right\} \qquad M(r) = -\frac{kT\,r}{G\mu m_p}\left\{\frac{d\ln\rho_g}{d\ln r}\right\}$$

$$\frac{\sigma_r^2 \mu m_p}{kT} \equiv \beta$$

- **If the gas distribution follows the matter distribution, and the latter follows an isothermal sphere model we get:**

$$\frac{\rho_g}{\rho_{g0}} = \left(\frac{\rho}{\rho_0}\right)^{\beta} \qquad \rho = \rho_0\left(1+\left(\frac{r}{r_c}\right)^2\right)^{-3/2} \qquad \rho_g = \rho_{g0}\left(1+\left(\frac{r}{r_c}\right)^2\right)^{-3/2\beta}$$

GAS DENSITY PROFILE

- **Fit to data finds $\beta \simeq 2/3$, but the β model provides a poor fit to disturbed systems**

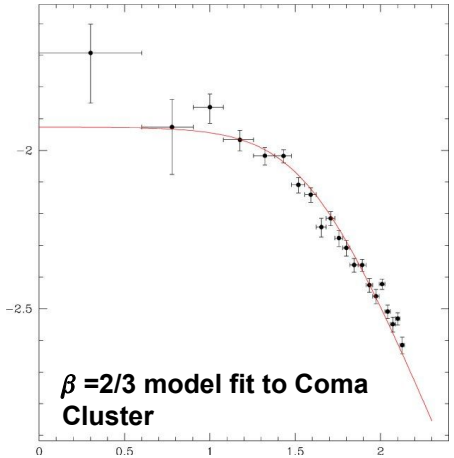

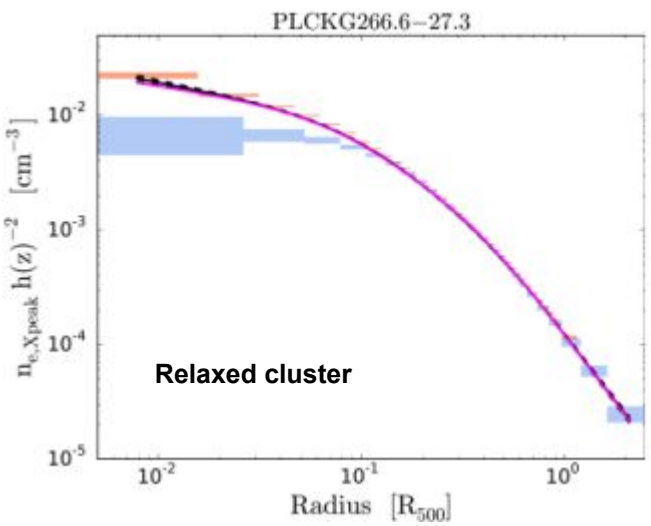

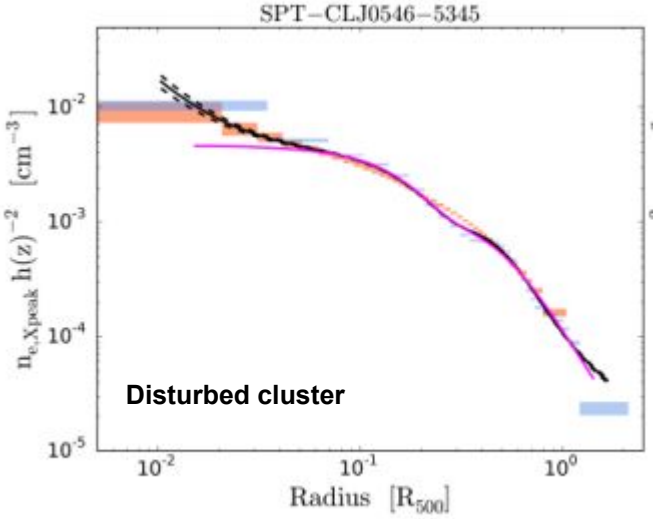

Bartalucci et al 2019

GAS DENSITY PROFILE

Vikhlinin et al 2006 model:

- **The β model is a poor description of the actual density profile; The shape of cluster density profiles is affected by the individual evolution history of the cluster (e.g. merging, AGN feedbacks)**
- **Vikhlinin introduced in 2006 a parametric model to account for the variegate cluster population**

$$n_p n_e = n_0^2 \frac{(r/r_c)^{-\alpha}}{\left(1+r^2/r_c^2\right)^{3\beta-\alpha/2}} \frac{1}{\left(1+r^\gamma/{r_s}^\gamma\right)^{\varepsilon/\gamma}} + \frac{n_{02}^2}{\left(1+r^2/r_{c2}^2\right)^{3\beta_2}}.$$

Term for the outskirts

Term accounting for the core

SURFACE BRIGHTNESS PROFILE

The gas density profile can be estimated from observations of the surface brightness.

- **Surface brightness: line-of-sight integral of the gas emissivity**

$$\varepsilon = n_e^2 \, \widetilde{\Lambda}(t) \quad \Rightarrow \quad S_x(R) = \frac{2}{4\pi} \int_R^\infty n_e^2 \, \widetilde{\Lambda}(t) \, dz$$

  - **Assuming a β model for the gas profile**

$$S_x(R) = \frac{n_{e0}^2 \widetilde{\Lambda}(t) \, r_c}{4\pi} \frac{\Gamma(0.5)\Gamma(3\beta - 0.5)}{\Gamma(3\beta)} \left(1 + \left(\frac{R}{r_c}\right)^2\right)^{-3\beta+1/2} (1+z)^{-4}$$

  - **Proportional to n_e^2 → Difficult to observe cluster outskirt**
  - **Proportional to $(1+z)^{-4}$ → Difficult to have high S/N X-ray observations at high redshift**

SURFACE BRIGHTNESS PROFILE

- **Spectrum from the center of a cluster:**

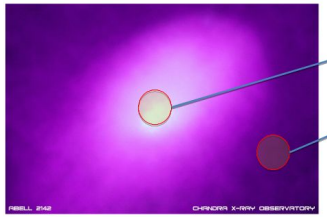

Black:data
Blue:background
Cyan: Bremstraulung + emission lines
Red: model fit

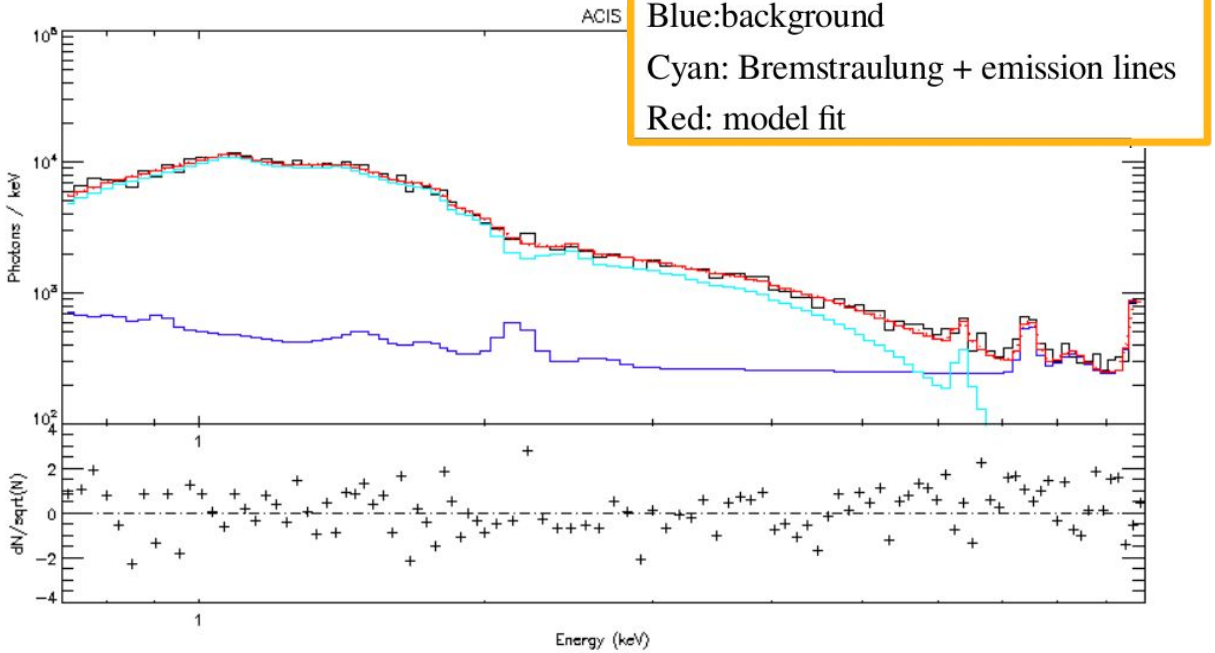

SURFACE BRIGHTNESS PROFILE

- **Spectrum from the outer regions of a cluster:**

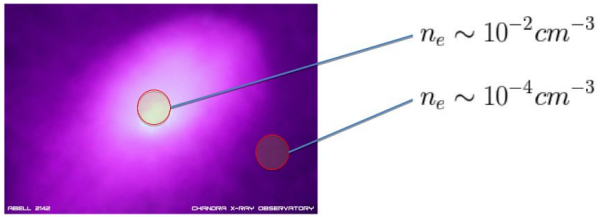

Black:data
Blue:background
Cyan: Bremstraulung + emission lines
Red: model fit

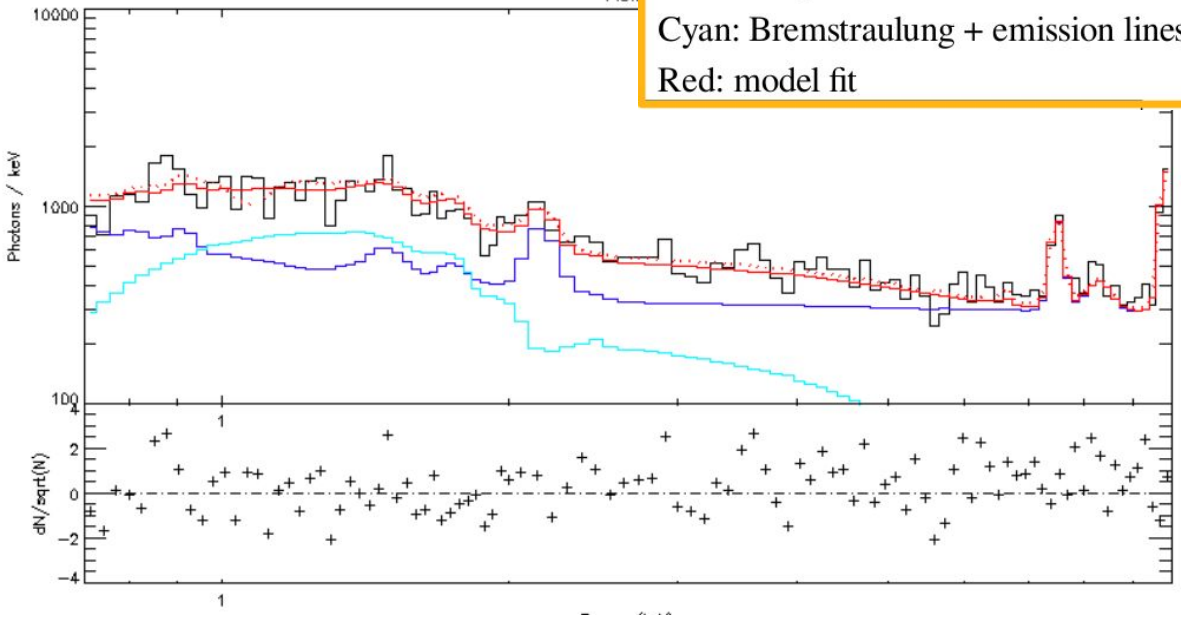

SURFACE BRIGHTNESS PROFILE

- **Surface brightness dimming:**

$$S_X \propto (1+z)^{-4}$$

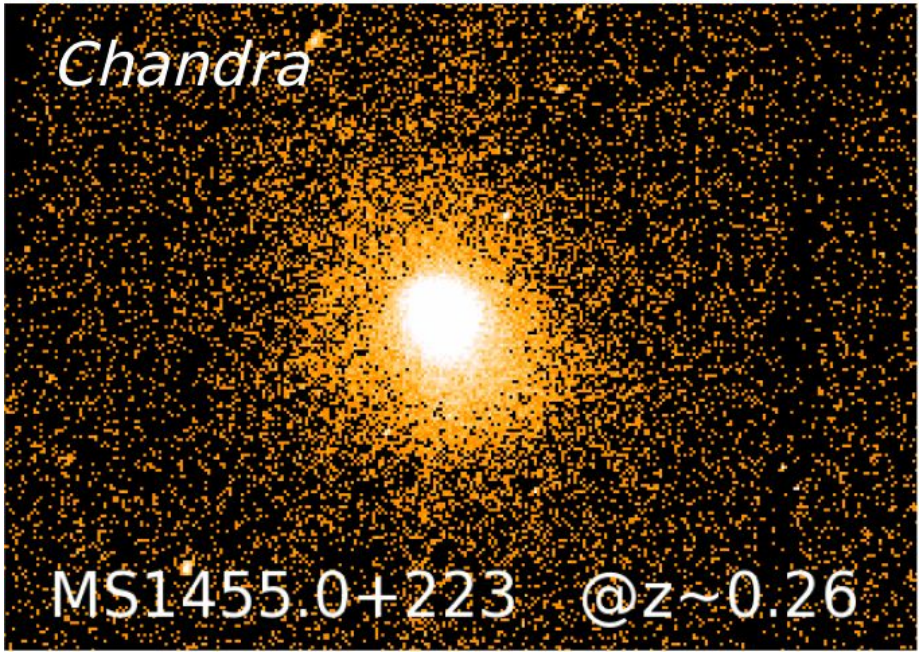

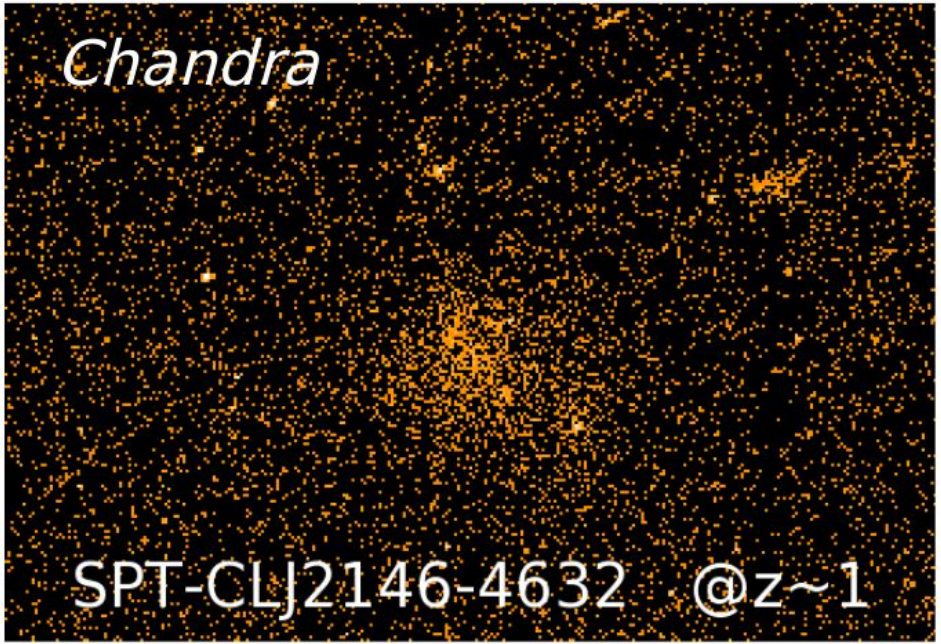

SURFACE BRIGHTNESS PROFILE

- **Surface brightness dimming:**

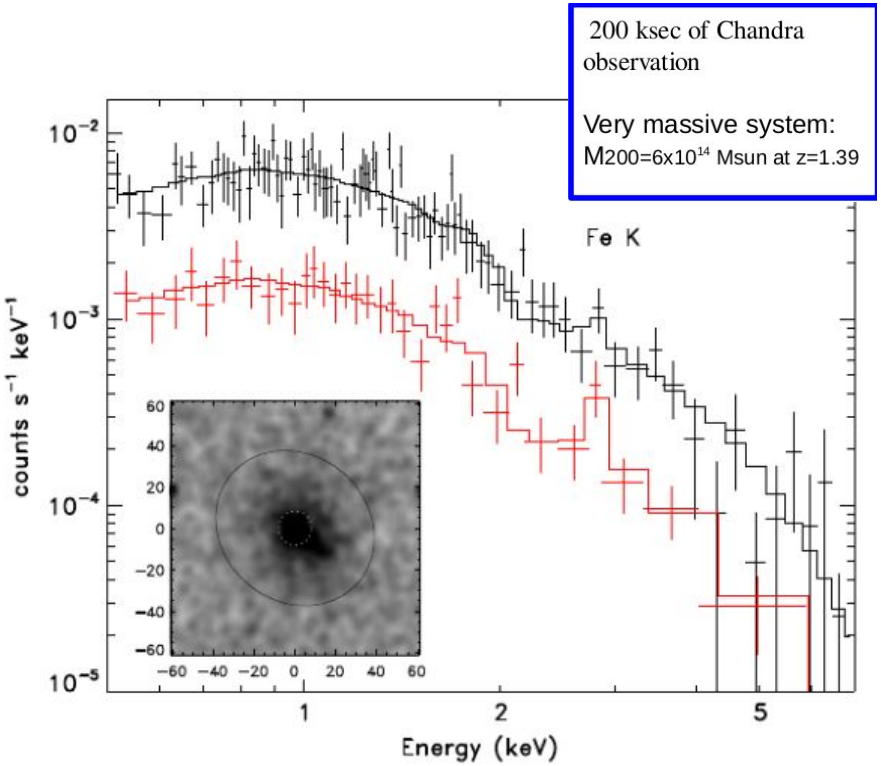

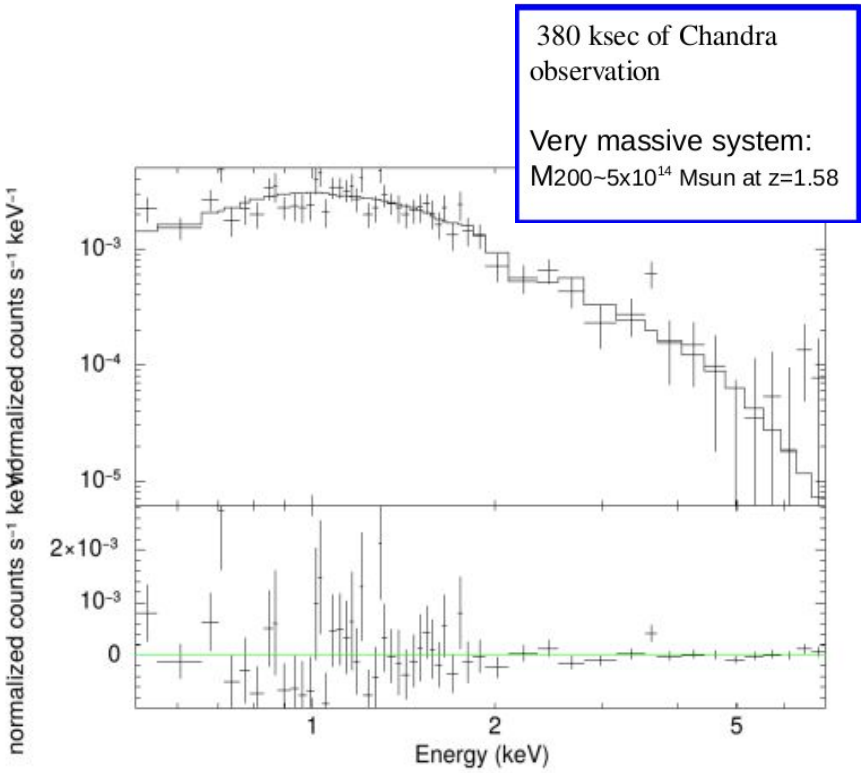

X-ray TELESCOPES

CHANDRA(NASA)

- Angular resolution: ~ 0.5 arcsec
- Energy range: [0.5-9] Kev
- Fov: ~ 16 arcmin

XMM-NEWTON(ESA)

- Angular resolution: ~ 6 arcsec
- Energy range: [0.3-10] Kev
- Fov: ~ 30 arcmin

X-ray TELESCOPES

Chandra

***A**dvanced **C**CD **I**maging **S**pectrometer*

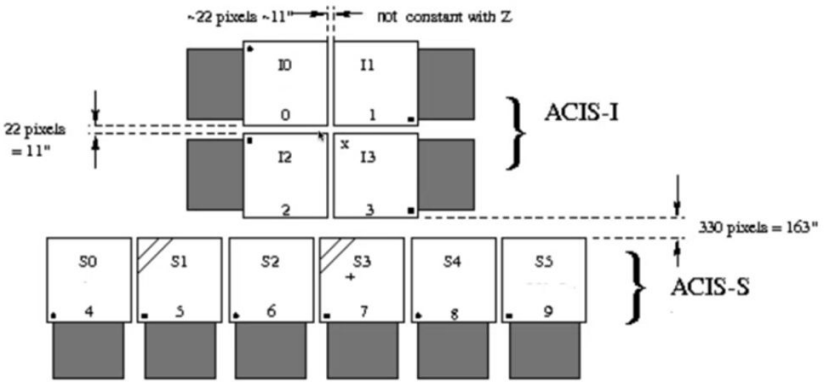

XMM-Newton

***E**uropean **P**hoton **I**maging **C**amera*

***M**etal **O**xide **S**emi-conductor* ***PN**-CCD*

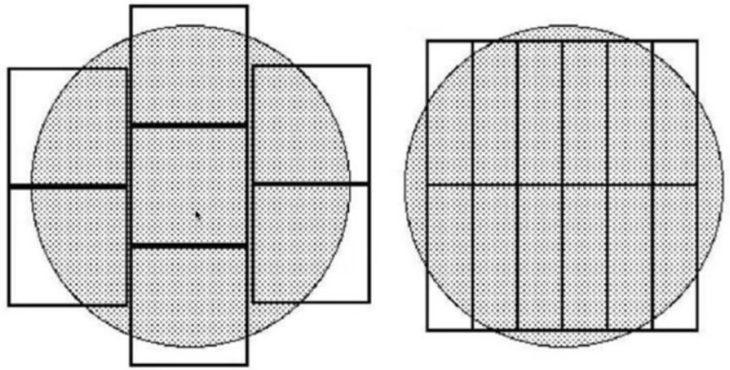

EPIC MOS

7 CCDs each 10.9 x 10.9 arcminutes

EPIC pn

12 CCDs each 13.6 x 4.4 arcmin

X-ray TELESCOPES

Instrument comparison:

- **Chandra: Higher resolution → Detection of substructures**
- **XMM: Higher sensitivity → cluster outskirt**

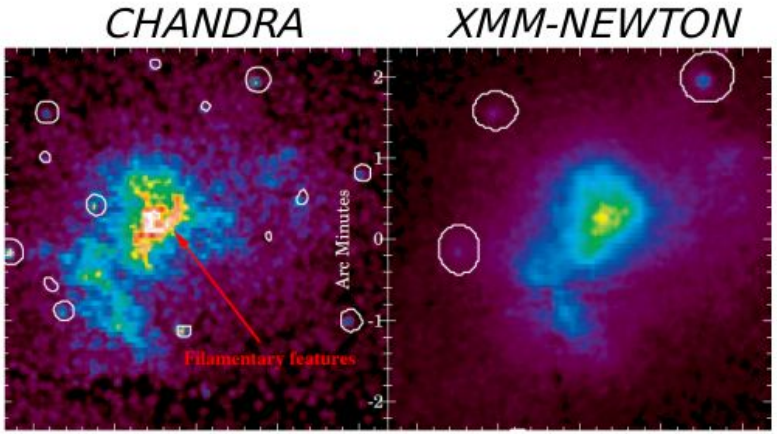

MACS J0717.5+3745
Z = 0.55

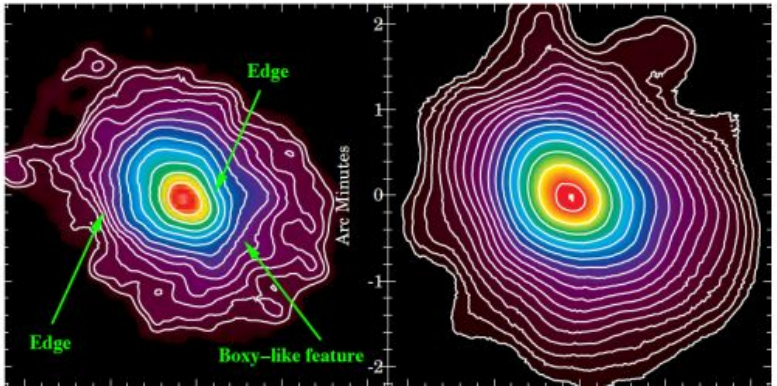

Cl0016+16
Z = 0.55

X-ray TELESCOPES

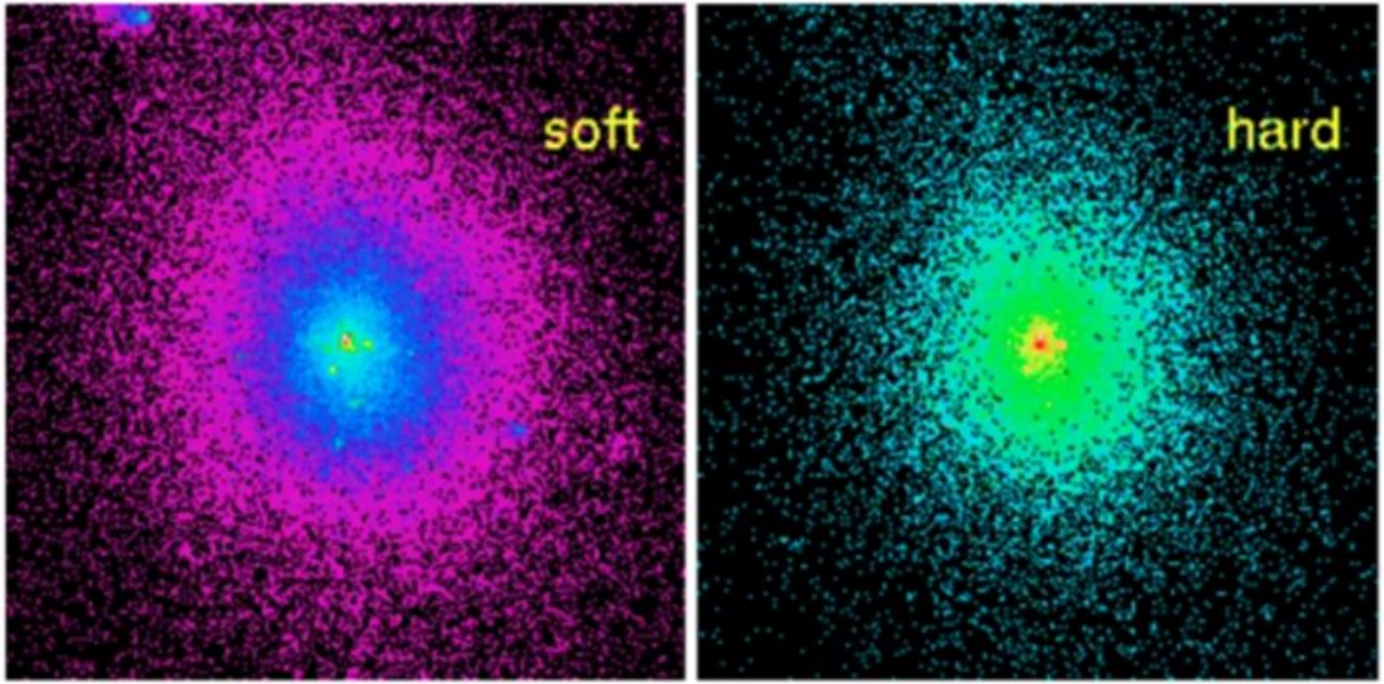

0.5-2 kev

2-7 kev

X-ray EVENT FILE

X-ray observations are available as a list of events, where an event is a list of informations for each detected photon.

XMM-NEWTON event file

	TIME	RAWX	RAWY	DETX	DETY	POS(X)	POS(Y)	PHA	PI	FLAG	PATTERN	CCDNR
units	s	PIXELS	PIXELS	pixel	pixel	pixel	pixel	CHAN	CHAN			
1	395587468.4	350	119	1084	-3995	26064	22332	3990	13069	4194304	0	1
2	395587468.4	570	164	5928	-3004	22021	19486	3989	13095	4194304	0	1
3	395587469.7	586	216	6281	-1865	20950	20010	3992	13118	4194304	0	1
4	395587468.2	511	242	4642	-1283	21650	21602	120	393	0	0	1
5	395587470.0	203	254	-2156	-1015	26117	26733	443	1477	0	0	1
6	395587472.1	366	399	1447	2175	21325	26299	425	1422	0	4	1
7	395587474.8	274	201	-592	-2198	25905	24784	520	1771	0	0	1
8	395587474.2	190	246	-2425	-1202	26438	26801	384	1274	0	0	1

time *position* *energy* *pattern*

X-ray BACKGROUND

X-ray background is formed by two main components:

- **Astrophysical:**
  - **X-ray emission from our own galaxy – Local Hot Bubble and hot gas in the galactic halo (e.g. Kuntz & Snowden 2000) modelled with two thermal emissions**
  - **Unresolved X-ray point sources (mostly AGNs) modelled with an absorbed power law (e.g. Lumb et al. 2002)**

- **Instrumental:**
  - **Emission from the telescope itself hit by high energetic particles (e.g. Hickox and Markevitch 2006)**
  - **Particles revealed by the detectors as photons**

SOURCE DETECTION

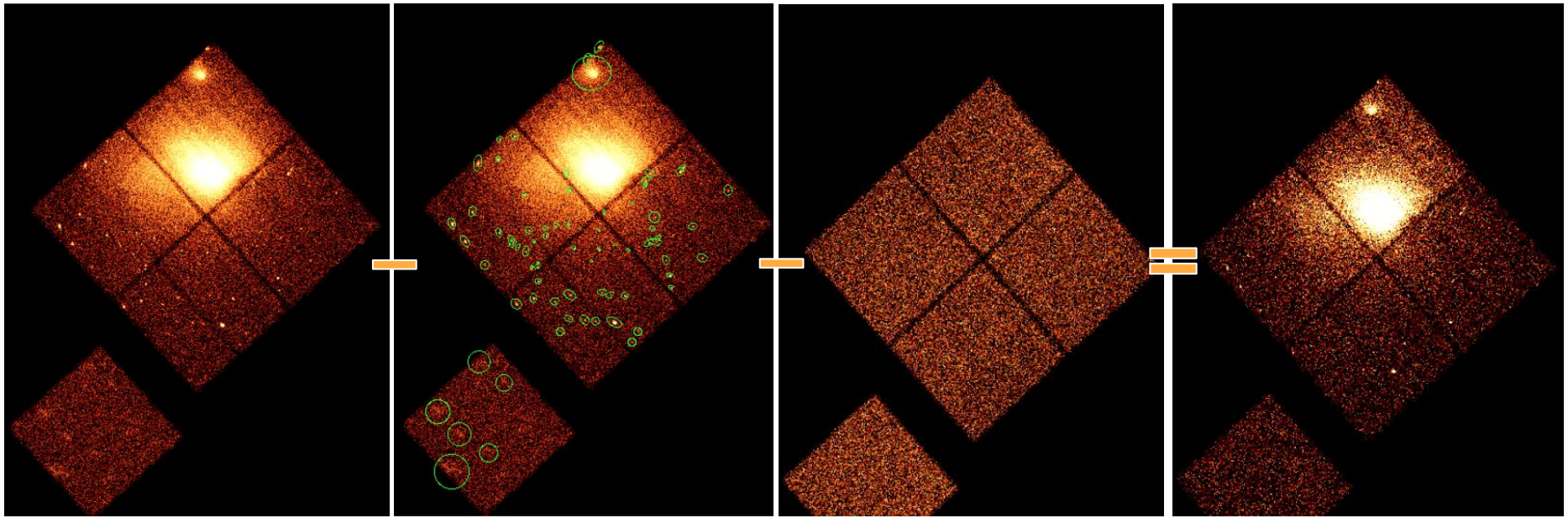

Flag all the resolved sources and mask them

Characterize and remove the background

Cluster detection

FITTING DENSITY AND TEMPERATURE PROFILES

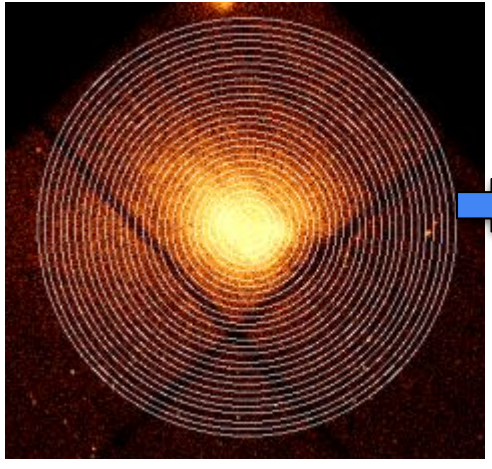

Measure the mean surface brightness in radial bins

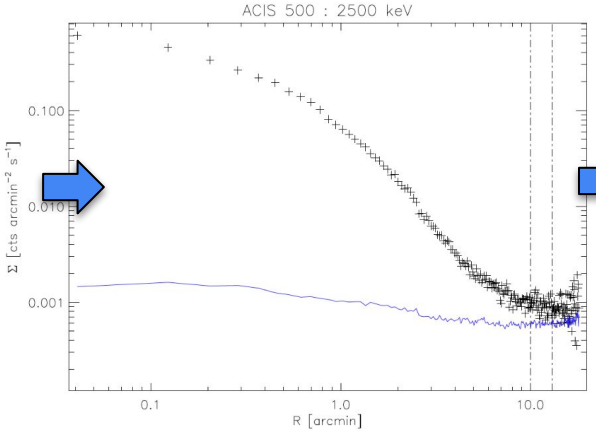

Fit the source brightness profile to derive the density profile

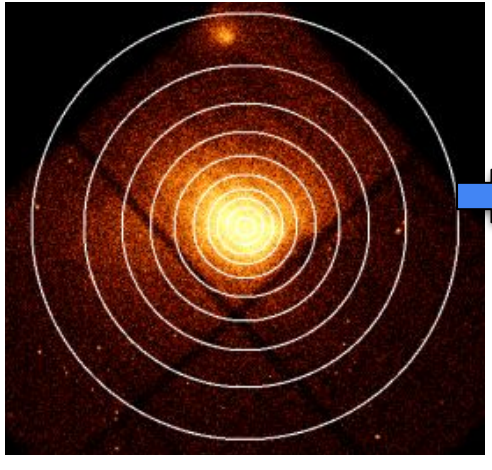

Measure the mean spectra in radial bins

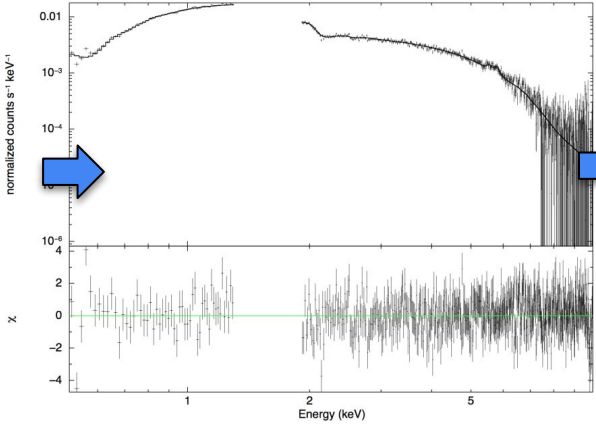

Fit the spectrum at each radial bin to derive the temperature profile

HYDROSTATIC MASS ESTIMATES

- **For a system in hydrostatic equilibrium the gravitational force is balanced by the outward pressure gradient**

$$\nabla P_{gas} = -\rho_{gas} \nabla \Phi$$

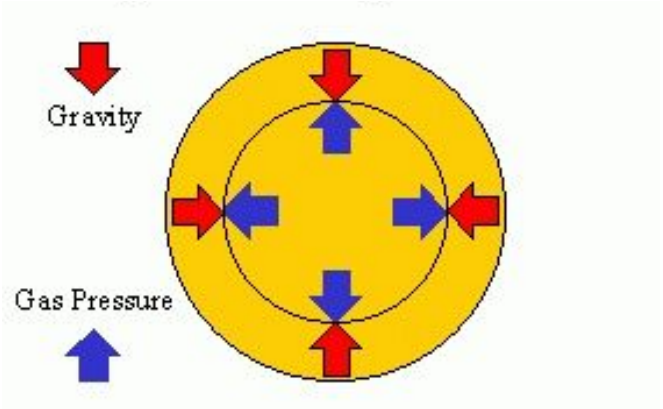

- **For a spherically symmetric system:**

$$\frac{dP}{dr} = -\rho_{gas} \frac{d\Phi}{dr} = -\rho_{gas} \frac{GM(r)}{r^2}$$

- **Including gas equation of state $P=nk_BT$, we can estimate the mass within the radius *r* as:**

$$M(r) = -\frac{r^2}{\rho_{gas}} \frac{dP}{dr} = -\frac{r}{G} \frac{kT}{\mu m_p} \left[\frac{dln\rho_{gas}}{dlnr} + \frac{dlnT}{dlnr} \right]$$

HYDROSTATIC MASS ESTIMATES

Five high redshift (z~1) clusters.

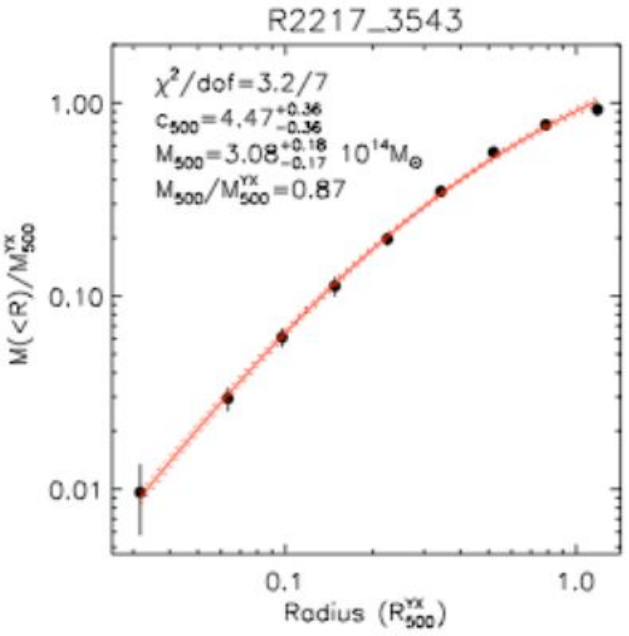

Credit: M. Arnaud

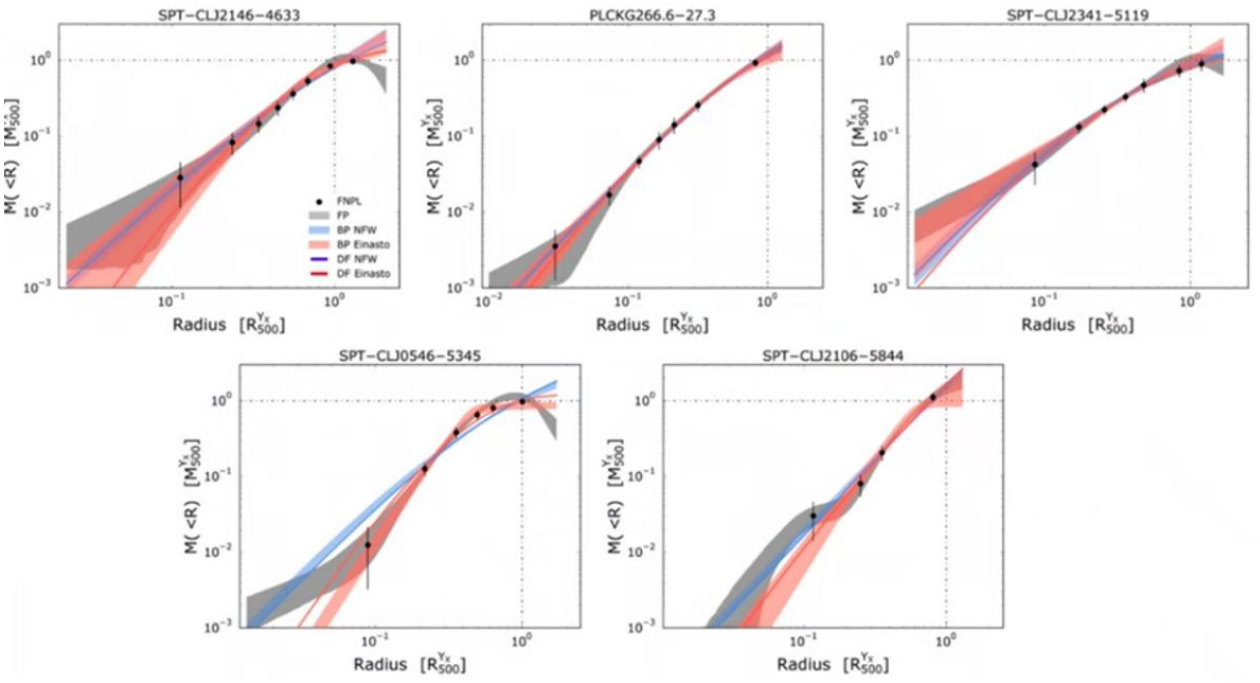

Bartalucci et al. 2018

HYDROSTATIC MASS ESTIMATES

- **The model assumes:**
  - **Hydrostatic equilibrium → (i.e. negligible non-thermal pressure support)**
  - **Spherical symmetry**

- **Both assumptions are ~met in relaxed systems. In disturbed/merging systems, turbulent motions provide extra pressure supports:**

$$\frac{\partial \boldsymbol{v}}{\partial t} + (\boldsymbol{v} \cdot \nabla)\boldsymbol{v} = -\frac{1}{\rho_{\rm gas}} \nabla P_{\rm gas} - \nabla \phi.$$

pressure profile of the Abell 2029 galaxy cluster derived from XRISM data https://arxiv.org/pdf/2505.06533

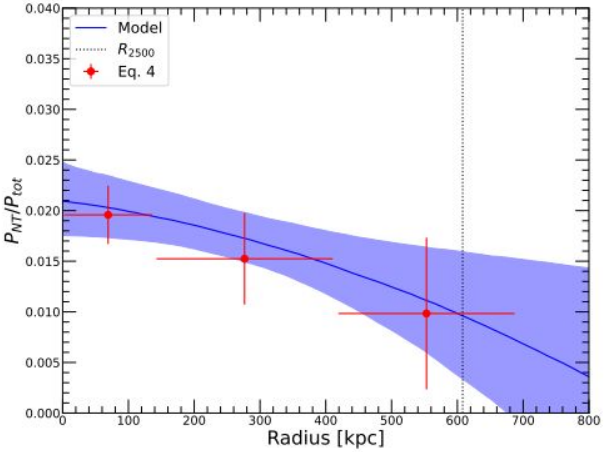

Fig. 6. Non-thermal pressure ratio as a function of cluster-centric radius inferred from the best-fit hydrostatic model (blue line and shaded area). The red data points show the non-thermal pressure ratio obtained directly from the Resolve data points through equation 4. The dashed vertical line shows the location of R_{2500}. Alt text: Line graph showing the pressure

HYDROSTATIC MASS BIAS

- **Ignoring the dynamical state of the cluster can lead to an underestimation of the mass (hydrostatic mass bias) of the order of 10-20%**

5 clusters in different dynamical state have been extracted from simulation and processed to obtain mock Chandra (ACIS-S3) long (1Ms) observations. (Rasia et al 2006)

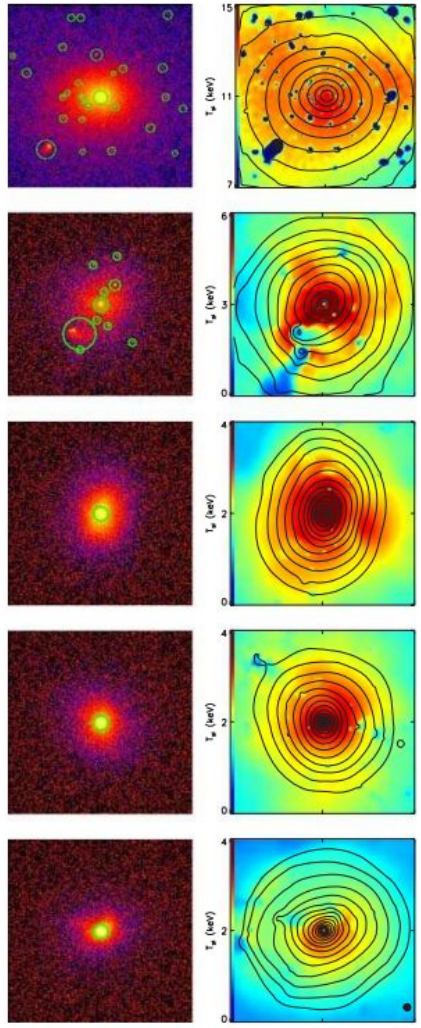

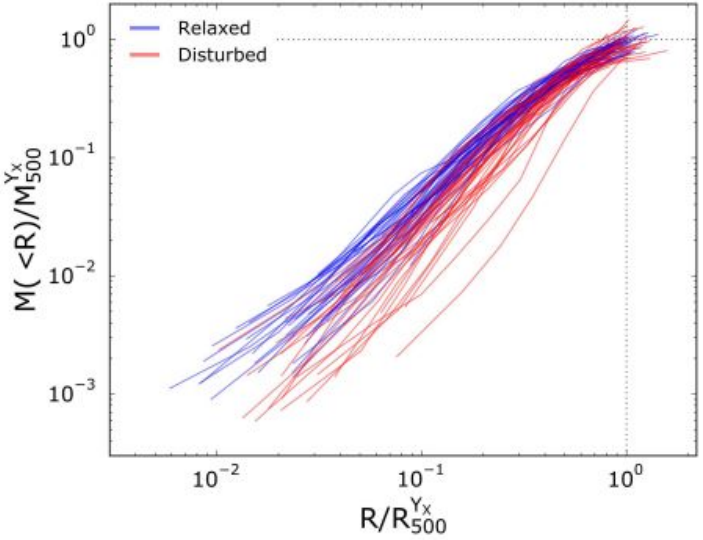

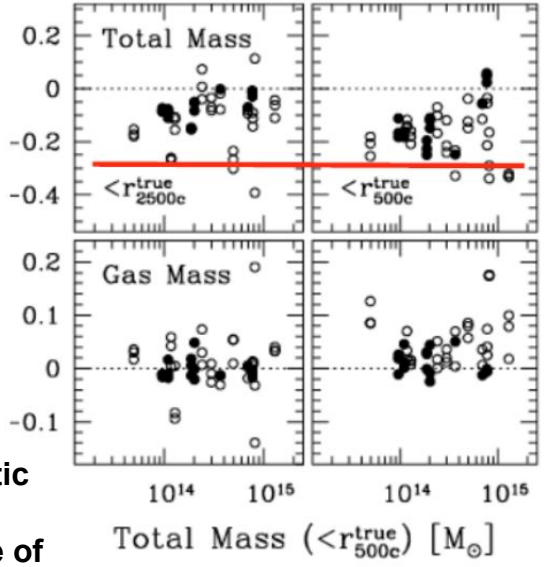

Scaled radial mass profiles extracted assuming hydrostatic equilibrium for 75 massive clusters; the mass profiles of disturbed systems (red) are consistently lower than those of relaxed systems (blue). Bartalucci et al 2019

HYDROSTATIC MASS

- Another source of uncertainty in the measurement of the profiles comes from the determination of the cluster center
- Two possible solutions are:
  - X-ray peak
  - X-ray centroid
- The difference between the two definition is larger for disturbed systems

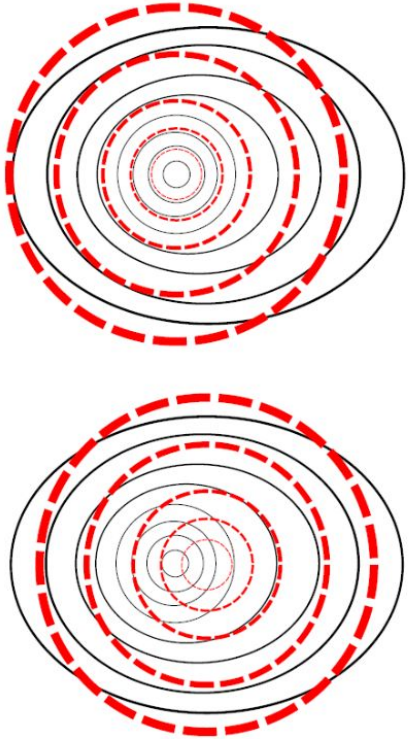

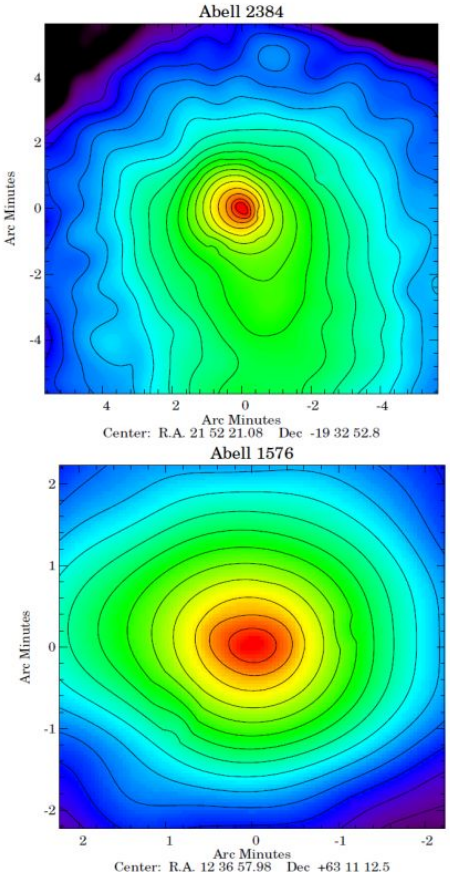

COOL CORE & NON-COOL CORE CLUSTERS

- **CC and non-CC systems have distinct physical signatures in their density, temperature, and metallicity profiles**

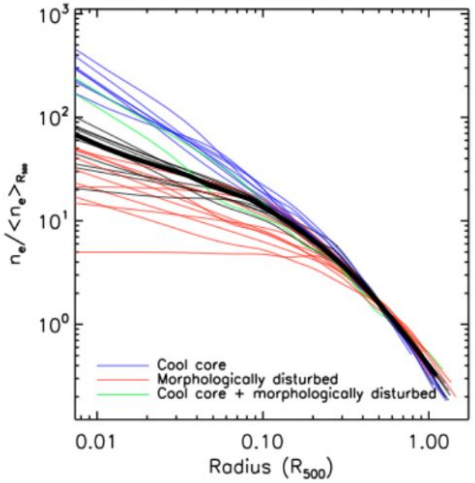

Arnaud et al. 2010

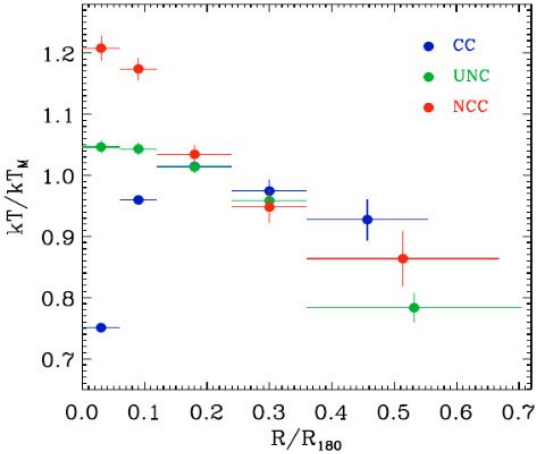

Leccardi et al. 2010

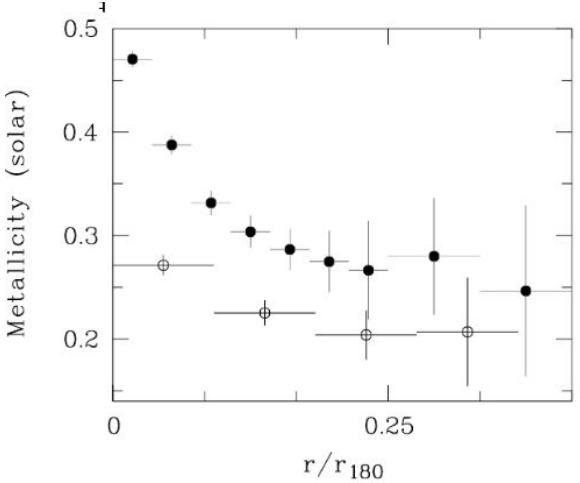

Leccardi et al. 2010

COOL CORE & NON-COOL CORE CLUSTERS

- **CC shows:**
  - **A larger density toward the center that triggers rapid X-ray cooling.**
  - **Temperature drops sharply in the center → The gas is losing energy faster than it can be replaced.**
  - **A strong central enrichment of metals (iron). The stable core allows metals from the central galaxy to accumulate.**
- **The CC and non-CC observations can be linked to the dynamical state of the cluster:**
  - **CC: relaxed systems where the central gas is dense enough to radiate away its energy via X-rays very efficiently. They are typically found in clusters that haven't experienced a major merger in billions of years.**
  - **non-CC: disturbed systems that have recently undergone a major merger with another cluster or group. The massive kinetic energy of the collision creates shocks and turbulence that "stir" the gas, injecting heat and erasing any pre-existing cool core. This results in a flatter, hotter, and more uniform central distribution.**

COOL CORE & NON-COOL CORE CLUSTERS

The Cooling Flow Problem:

- **Based on X-ray observations, the hot, dense gas in the center of these clusters should radiate X-rays, lose energy, and cool down rapidly to low temperatures ($<10^4$ K), resulting in massive "cooling flows" of gas falling onto the central galaxy (rates of 100–1000 $M_\odot$/yr)**
- **X-ray spectroscopy shows that while the gas is indeed cooler in the center, it does not cool below a certain temperature threshold (T ~ 10^7 K). The expected large masses of cold (T< 10^4K) gas and high star formation rates are largely absent, with observations revealing a cooling rate that is ~5 times less than predicted**
- **The primary resolution to the paradox is that the gas is being continuously heated, likely by the central supermassive black hole's active galactic nucleus (AGN) feedback, which balances the radiative cooling; jets from the AGN pumps just enough energy back into the gas to keep it from collapsing completely, maintaining equilibrium.**

COOL CORE & NON-COOL CORE CLUSTERS

Selection effects:

- **Due to the n_e^2 dependency of the surface brightness, CC systems are more easily detected in X-ray surveys.**
- **This selection effect needs to be properly modeled for the cosmological exploitation of X-ray catalogs**

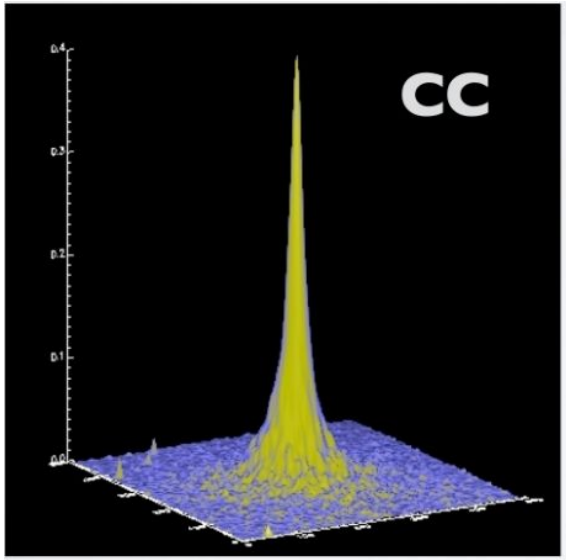

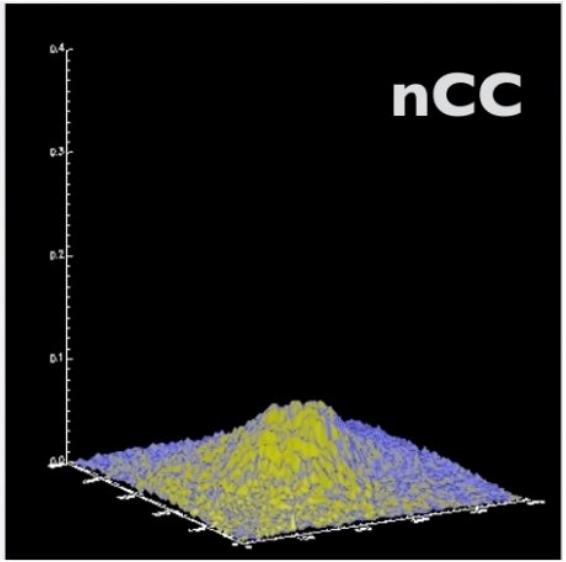

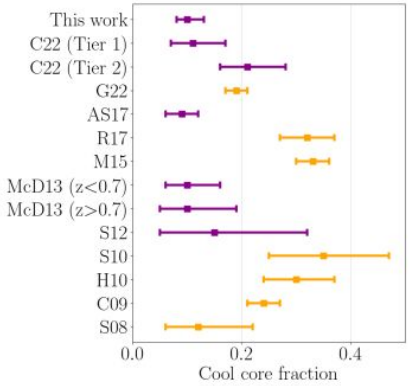

Figure 6. A comparison of the cool core fraction calculated using surface brightness concentration for the CE-REAL sample compared to the literature. For this figure, we define cool core systems as those with strong cool cores ($c_{SB,\,phys} > 0.155$), and all errorbars are 1σ confidence intervals calculated using binomial probabilities. For CHEX-MATE, we convert the $c_{SB,\,phys}$ threshold to a $c_{SB,\,scaled}$ threshold using the best-fit line from Figure 4. For any samples which use cool core proxies other than c_{SB}, such as central entropy, we use relations from Hudson et al. (2010) to convert to c_{SB} and apply the same cut. The referenced samples are: CHEX-MATE Tier 1 and Tier 2 (C22; Campitiello et al. 2022), eFEDS (G22; Ghirardini et al. 2022), AS17 (Andrade-Santos et al. 2017), MACS (R17; Rossetti et al. 2017), M15 (Mantz et al. 2015), McD13 (McDonald et al. 2013), S12 (Semler et al. 2012), 400D (S10; Santos et al. 2010), HIFLUGCS (H10; Hudson et al. 2010), ACCEPT (C09; Cavagnolo et al. 2009), and S08 (Santos et al. 2008). The point types are color-coded with orange corresponding to X-ray selection and purple corresponding to SZ selection. In general, the cool core fraction tends to agree between publications that use the same cluster selection.

https://arxiv.org/pdf/2603.06785

ATHENA X-ray TELESCOPE

Observation of the Chandra Deep field South with Athena and Chandra

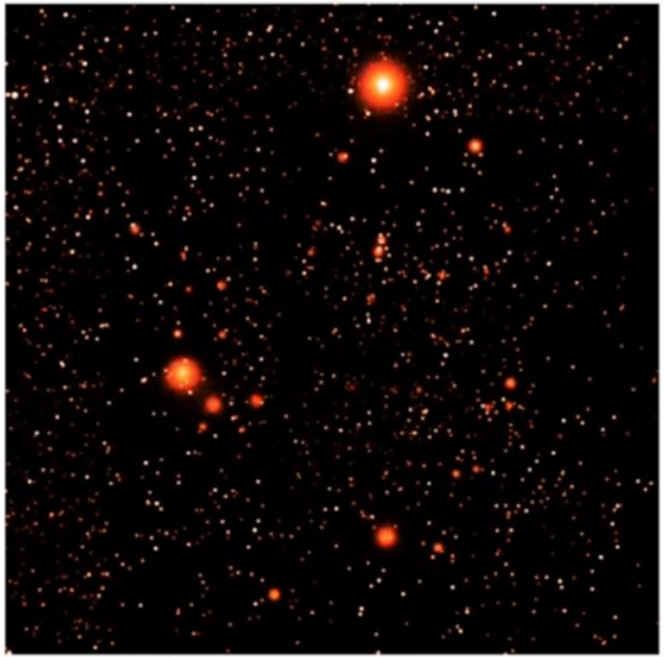

Athena simulated image:
40x40 arcmin 130 hours observation

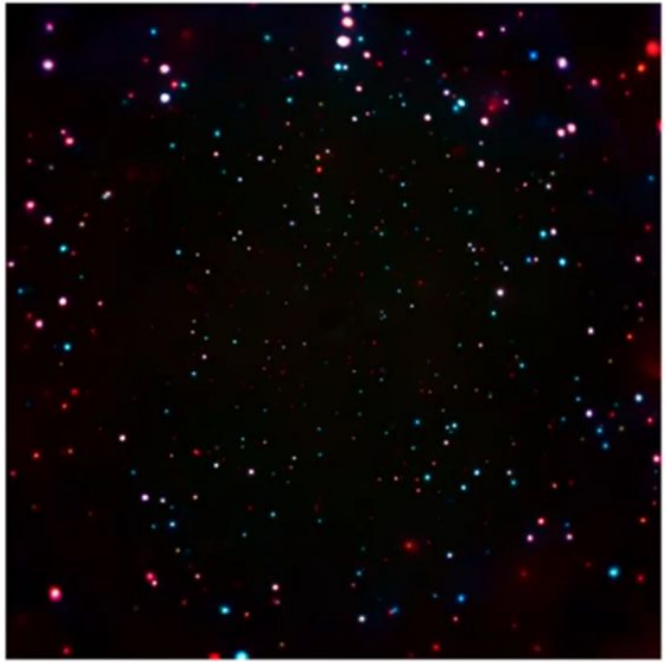

Chandra image:
16x16 arcmin 2000 hours observation

With Athena we see more objects with larger larger FOV with ~1/20 of observation time

ATHENA X-ray TELESCOPE